

## Breakdown of compensation and persistence of nonsaturating magnetoresistance in gated WTe<sub>2</sub> thin flakes

Yilin Wang,<sup>1,3</sup> Kefeng Wang,<sup>1</sup> Janice Reutt-Robey,<sup>3</sup> Johnpierre Paglione,<sup>1</sup> and Michael S. Fuhrer<sup>1,2,\*</sup>

<sup>1</sup>*Department of Physics, Center for Nanophysics and Advanced Materials, University of Maryland, College Park, Maryland 20742, USA*

<sup>2</sup>*School of Physics, Monash University, Victoria 3800, Australia*

<sup>3</sup>*Department of Chemistry and Biochemistry, University of Maryland, College Park, Maryland 20742, USA*

(Received 6 October 2015; revised manuscript received 7 March 2016; published 22 March 2016)

The recently discovered large nonsaturating magnetoresistance in semimetal WTe<sub>2</sub> may result from near-perfect electron-hole compensation, however recent reports question whether the compensation is adequate to explain the observations. Experiments on significantly uncompensated WTe<sub>2</sub> are needed. We measure magnetoresistance  $\rho_{xx}(H)$ , Hall effect  $\rho_{xy}(H)$ , and an electrolyte gating effect in thin (<100 nm) exfoliated WTe<sub>2</sub>. We observe  $\rho_{xy}(H)$  linear in  $H$  at low  $H$  consistent with near-perfect compensation, however  $\rho_{xy}(H)$  becomes nonlinear and changes sign with increasing  $H$ , implying a breakdown of compensation. We break compensation more significantly by using an electrolytic gate for highly electron-doped WTe<sub>2</sub> with Li. In gated WTe<sub>2</sub> the nonsaturating  $\rho_{xx}(H)$  persists to  $H = 14$  T, even with significant deviation from perfect electron-hole compensation ( $p/n = 0.84$ ) where the two-band model predicts a saturating  $\rho_{xx}(H)$ . Our results indicate electron-hole compensation is not the mechanism for extremely large magnetoresistance in WTe<sub>2</sub>; alternative explanations are needed.

DOI: [10.1103/PhysRevB.93.121108](https://doi.org/10.1103/PhysRevB.93.121108)

After the successful exfoliation of single layer graphene in 2004, two-dimensional layered materials, such as transition-metal dichalcogenides (TMDCs), are under intense study due to their excellent electrical, optical, thermal, and mechanical properties [1]. Among TMDCs, semimetal tungsten ditelluride (WTe<sub>2</sub>) has attracted significant research interest since the recent discovery of its extremely large nonsaturating magnetoresistance (XMR) [2], which could find potential applications in magnetic memory and sensing. The XMR in WTe<sub>2</sub> is believed to arise from perfect compensation of electron ( $n$ ) and hole ( $p$ ) carrier densities [2], similar to the case observed in high-purity graphite and bismuth [3]; this is supported by angle-resolved photoemission spectroscopy (ARPES) experiments, which observed nearly identical sized electron and hole pockets [4]. These results have been complicated by further ARPES study [5], which revealed a more complicated Fermi surface, and transport studies of Shubnikov-de Haas (SdH) quantum oscillations [6,7], which reflect the existence of four Fermi pockets. The application of pressure, which increases the difference between electron and hole pockets, suppresses the magnetoresistance [8–10], further supporting the electron-hole compensation scenario. However the origin of XMR in WTe<sub>2</sub> is still unclear and remains under discussion [5,7], therefore more experiments to measure [11] and tune the degree of compensation are highly desired to clarify this important issue.

In this Rapid Communication, we present detailed temperature- and gate-dependent magnetoresistivity  $\rho_{xx}(H)$  and Hall resistivity  $\rho_{xy}(H)$  measurements on exfoliated WTe<sub>2</sub> thin (<100 nm) flakes in an attempt to reveal the relationship between magnetoresistivity and electron and hole concentrations. We observe quantum oscillations in both  $\rho_{xx}(H)$  and  $\rho_{xy}(H)$  with four oscillation frequencies resolved in the fast Fourier-transform analysis, consistent

with earlier reports [6,7]. Hall resistivity exhibits pronounced temperature-dependent nonlinear behavior and changes its sign under a magnetic field; the nonlinearity is strong evidence of a breakdown in the perfect electron-hole compensation. By fitting the Hall resistivity with a two-band model, we found the two carriers are well compensated under a low field where  $\rho_{xy}(H)$  is linear in  $H$ ; although they are not compensated under a high field, holes have the larger carrier population and electrons show higher mobility. We also tuned the doping and compensation ratio  $p/n$  through electrolyte gating. We find that the large nonsaturating magnetoresistivity persists, up to  $2 \times 10^4$  % at  $H = 14$  T, even though the electrons and holes become significantly uncompensated with  $p/n$  as small as 0.84. For such uncompensated samples, a two-band model predicts a saturating magnetoresistivity not seen in experiment. The results indicate that near-perfect electron-hole compensation is not required for nonsaturating magnetoresistance and suggests alternative explanations need to be explored.

The Fig. 1(a) inset shows a typical optical image of one of our WTe<sub>2</sub> devices with a thickness of about 70 nm. WTe<sub>2</sub> is found to have a distorted-1T structure with tungsten chains sandwiched between two layers of tellurium atoms, which makes it cleave easily into atomically thin layers [12]. WTe<sub>2</sub> thin flakes are obtained by mechanical exfoliation of ribbonlike single crystals on a 300 nm SiO<sub>2</sub>/Si substrate. Single-crystal platelets of WTe<sub>2</sub> were grown via the high-temperature self-flux method. High-purity elemental W and Te in a W/Te = 1/49 ratio were placed in the alumina crucible which was sealed in a quartz tube. The sealed tube was heated to 1000 °C and then slowly cooled down to 480 °C where the residual Te flux was decanted with a centrifuge. Figure S1 [13] shows the x-ray-diffraction pattern of a powdered sample and a cleaved surface of a WTe<sub>2</sub> bulk single crystal, indicating its high quality. The electrical contacts are defined with standard electron-beam lithography and thermally evaporated Cr/Au (5 nm/100 nm). The Hall bar geometry is defined via SF<sub>6</sub>

\*michael.fuhrer@monash.edu

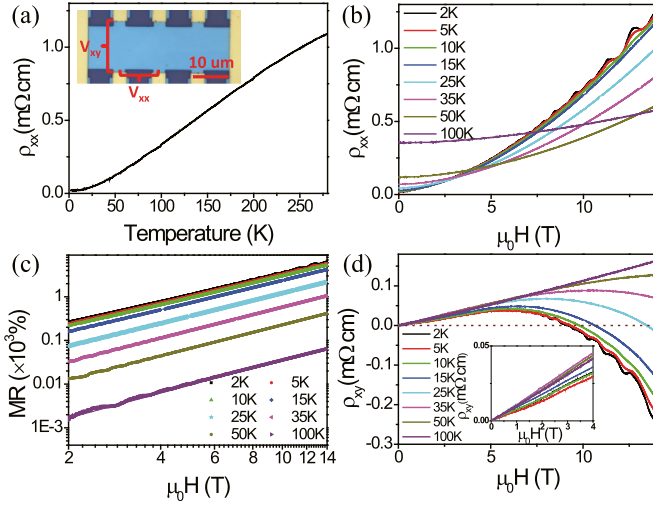


FIG. 1. (a) Temperature-dependent resistivity  $\rho_{xx}$  of WTe<sub>2</sub> thin flakes at zero magnetic field. The inset shows the typical optical image of our WTe<sub>2</sub> devices with Hall-bar geometry. (b) Magnetic-field dependence of resistivity  $\rho_{xx}(H)$  at various temperatures indicated in the legend. (c) Magnetoconductance ratio (MR) vs field in a log-log plot; straight lines indicate a power-law relationship  $MR \sim H^n$ . (d) Magnetic-field dependence of the Hall resistivity  $\rho_{xy}(H)$  at various temperatures indicated in the legend. The inset shows the same data at low magnetic fields.

plasma etching. Four-probe measurements of magnetoresistivity and Hall resistivity were conducted by lock-in techniques at a low frequency of 3.7 Hz and in a commercial cryostat (Quantum Design PPMS-14). The Hall voltage was recorded in both polarities of the magnetic field and antisymmetrized to remove longitudinal voltage components. The polymer electrolyte was prepared by dissolving the mixture of LiClO<sub>4</sub> and polyethylene oxide in the weight ratio of 0.12:1 in methanol and then stirring overnight at room temperature [14].

Figure 1(a) shows the temperature-dependent resistivity  $\rho_{xx}(T)$  of this device at  $H = 0$ ; the resistivity decreases monotonically with decreasing temperature, exhibiting metallic behavior. A residual resistance ratio of 55 is observed. In Fig. 1(b), which presents the magnetic-field-dependent resistivity  $\rho_{xx}(H)$  with  $H \parallel c$  at various temperatures, the resistivity increases monotonically with increasing magnetic field with no sign of saturation up to 14 T. Clear SdH quantum oscillations are also observed below 10 K. These results are similar to those reported for bulk single crystals [2,6–8,15]. Figure 1(c) shows the MR,  $MR = [\rho(H) - \rho(0)]/\rho(0)$  as a function of magnetic field in a log-log plot at various temperatures; the linear dependence indicates power-law  $MR \sim H^n$  behavior with  $n = 1.6$  at  $T = 2$  K and gradually increasing to  $n = 1.9$  at  $T = 100$  K [16].

Figure 1(d) shows the field-dependent Hall resistivity  $\rho_{xy}(H)$  measured at various temperatures ( $\rho_{xx}(T)$ , MR and  $\rho_{xy}(H)$  on bulk crystal are shown in Supplemental Material Fig. S2 [13]). At temperatures below 50 K,  $\rho_{xy}(H)$  exhibits nonlinear behavior, whereas at temperatures above 100 K,  $\rho_{xy}(H)$  behavior is quite linear. At low fields,  $\rho_{xy}$  is positive with a value that depends nearly linearly on field; with increasing field, the slope gradually changes from positive to negative, and  $\rho_{xy}$  changes its sign. With increasing temperature, the

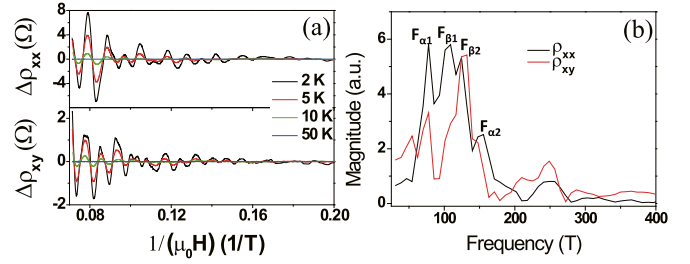


FIG. 2. (a) Quantum oscillations of the longitudinal resistivity (SdH, upper panel) and Hall resistivity (lower panel) after subtraction of a polynomial background at various temperatures. (b) Fast Fourier transform of the quantum oscillations of  $\rho_{xx}$  and  $\rho_{xy}$  vs  $1/H$  at  $T = 2$  K; four oscillation frequencies are resolved as denoted on the plot.

field where  $\rho_{xy}$  changes the sign continuously increases. (The nonlinear behavior of Hall resistivity was confirmed in several devices, see Supplemental Material Fig.S3 [13].) These features are similar to that of other XMR materials, such as NbSb<sub>2</sub> [17] and definitely indicate multiple Fermi pockets; at least two types of carriers play a role in the transport properties of WTe<sub>2</sub>. Notably, the nonlinearity of  $\rho_{xy}$  within a two-band model occurs only if the two carrier densities are unequal [17,18]. A detailed analysis of  $\rho_{xy}(H)$  will be presented below. At 2 K and high fields ( $> 5$  T), clear quantum oscillations superimposed on the smooth background were observed.

Quantum oscillations of magnetoresistivity and Hall resistivity are obtained by subtracting the smoothly varying background fitted to a polynomial and are shown in Fig. 2(a) at various temperatures. The amplitude of the quantum oscillations of both  $\rho_{xx}(H)$  and  $\rho_{xy}(H)$  decreases with increasing  $T$ , and the oscillations are not observed for  $T > 15$  K. In order to resolve the frequency of quantum oscillations, a Fourier-transform analysis was carried out on  $\rho_{xx}$  vs  $1/H$  with results shown in Fig. 2(b). Four major peaks at frequencies  $F_{\alpha 1} = 78$  T,  $F_{\beta 1} = 105$  T,  $F_{\beta 2} = 124$  T, and  $F_{\alpha 2} = 151$  T were identified, which may correspond to four distinct Fermi pockets ( $F_{\alpha}$  and  $F_{\beta}$  correspond to previously observed hole and electron pockets, respectively) [6,7]. Fourier-transform analysis of  $\rho_{xy}$  vs  $1/H$  [the red curve in Fig. 2(b)] shows similar oscillation frequencies as the SdH oscillations. The observation of SdH oscillations with accompanying quantum Hall oscillations suggests the Landau levels in this system are well resolved, indicating the high quality of the device.

In order to further analyze  $\rho_{xx}(H)$  and  $\rho_{xy}(H)$  in WTe<sub>2</sub>, we adopt a two-band model [19],

$$\rho_{xx} = \frac{1}{e} \frac{(n\mu + p\mu') + (p\mu + n\mu')\mu\mu'H^2}{(n\mu + p\mu')^2 + [(p - n)\mu\mu'H]^2}, \quad (1)$$

$$\rho_{xy} = \frac{1}{e} \frac{(n\mu^2 - p\mu'^2) - (p - n)\mu^2\mu'H^2}{(n\mu + p\mu')^2 + [(p - n)\mu\mu'H]^2} H, \quad (2)$$

where  $n(p)$  and  $\mu(\mu')$  are the carrier density and mobility for electrons (holes), respectively, and  $H$  is the magnetic field. Recent experiments indicate that WTe<sub>2</sub> may have more than two Fermi surfaces, however the two-band model is the simplest model that captures the physics of nonsaturating MR due to compensation. The addition of more carrier types to the model might produce a better fit to the data however would

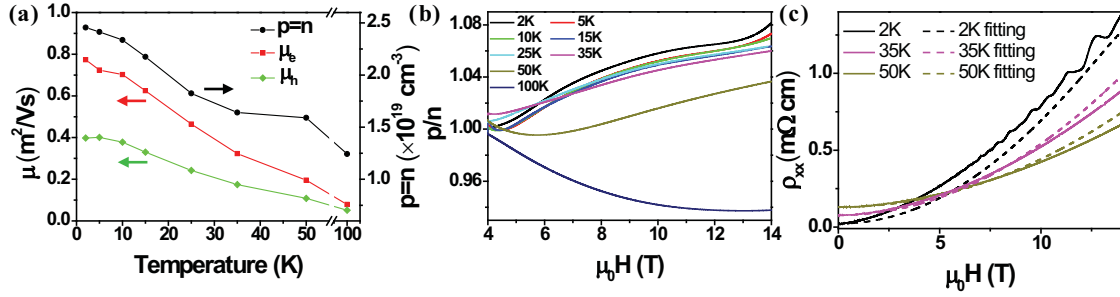


FIG. 3. (a) The mobilities  $\mu$  ( $\mu'$ ), and carrier densities  $p = n$  of electrons and holes at various temperatures, extracted from data in Figs. 1(b) and 1(d) at  $H < 4$  T. (b) The  $p/n$  ratio as a function of magnetic field at various temperatures shown in the legend, determined from data in Fig. 1(d) using Eq. (2) as described in the text. (c) Experimental  $\rho_{xx}(H)$  (solid lines) and predicted  $\rho_{xx}(H)$  (dashed lines) using parameters from (a) and (b) at three representative temperatures as indicated in legend.

not change the general conclusions. Notably nonsaturating MR requires perfect compensation in the classical model.

The  $\rho_{xy}(H)$  at a low field ( $< 4$  T) is linear (slope independent of  $H$ ), indicating  $p = n$ , i.e., the electrons and holes are well compensated at a low field. The slope of  $\rho_{xy}(H)$  at a high field is nonlinear and strongly field dependent, which is inconsistent with Eqs. (1) and (2) with  $p = n$ ; the two-band model cannot explain  $\rho_{xy}(H)$  with fixed parameters  $n, p, \mu$ , and  $\mu'$ . Indeed, recent density functional theory calculations including spin-orbit coupling predict the Fermi surface of  $\text{WTe}_2$  exhibit a strong magnetic-field-dependent behavior because of the Zeeman effect and the hole pockets change significantly when the Fermi level is displaced by a small amount of energy [7]. Since the nonlinearity of  $\rho_{xy}(H)$  is highly suggestive that electrons and holes are not well compensated, i.e.,  $p \neq n$ , the simplest modification to the two-band model is to adopt a dependence of the ratio  $p/n$  on  $H$  as follows. The combined linear fitting of  $\rho_{xy}(H)$  and second-order polynomial fitting of  $\rho_{xx}(H)$  at a low field ( $< 4$  T) with the two-band model Eqs. (1) and (2) with  $p = n$  yields mobility ( $\mu$  and  $\mu'$ ) and both carrier densities. Figure 3(a) shows the extracted mobilities and carrier densities at various temperatures; at 2 K,  $p = n = 2.45 \times 10^{19} \text{ cm}^{-3}$ ,  $\mu = 0.77 \text{ m}^2 \text{ V}^{-1} \text{ s}^{-1}$ , and  $\mu' = 0.40 \text{ m}^2 \text{ V}^{-1} \text{ s}^{-1}$ , and  $p, n, \mu$ , and  $\mu'$  gradually decrease with increasing temperature. The electron and hole densities are consistent with the previously reported results [6]. We then assume that the nonlinearity of  $\rho_{xy}(H)$  for  $H > 4$  T is attributed entirely to the variation of the  $p/n$  ratio; we fix  $\mu, \mu'$ , and  $p + n$  by their

low-field values. Figure 3(b) shows the  $p/n$  ratio as a function of magnetic field at various temperatures. The  $p/n$  ratio varies continuously with field and gives consistent results at every temperature from  $2 \text{ K} \leq T \leq 35 \text{ K}$ . As a check we use the  $p/n$  ratio in Fig. 3(b) together with  $\mu, \mu'$ , and  $p + n$  to predict  $\rho_{xx}(H)$  using Eq. (1) as shown in Fig. 3(c). The predicted  $\rho_{xx}(H)$  is in reasonable agreement with experiment. We note that better agreement could be obtained by allowing  $\mu$  ( $\mu'$ ), and/or  $p + n$  to vary as well. The variation of  $\rho_{xy}$  with  $H$  could in principle be explained with  $p = n$  however it would require drastic variation in  $\mu$  and  $\mu'$ , including a change in relative magnitude, which we find much less likely especially in a scenario that conserved  $p = n$ . Hence the nonlinear  $\rho_{xy}(H)$  provides strong evidence that near-perfect compensation does not survive to high  $H$ . The  $p/n$  ratio is slightly above 1 below 50 K at  $H > 4$  T, indicating the concentration of holes is higher than that of electrons; the mobility of holes is smaller ( $\sim 50\%$ ) than that of electrons. The higher carrier population and lower mobility of holes give rise to the sign reversal of  $\rho_{xy}$  in a magnetic field at low temperature. The carrier mobility is above the threshold value for observation of quantum oscillations in magnetoresistivity and Hall resistivity:  $\mu B \approx 1$ . At 100 K, we find a  $p/n$  ratio smaller than 1, indicating the concentration of electrons is higher than that of holes, which is consistent with the observation via ARPES experiments of increased electron doping due to thermal activation above 100 K [4] (albeit at  $H = 0$ ).

We also used an electrolyte gate to tune the absolute and relative densities of electrons and holes in  $\text{WTe}_2$  thin crystals.

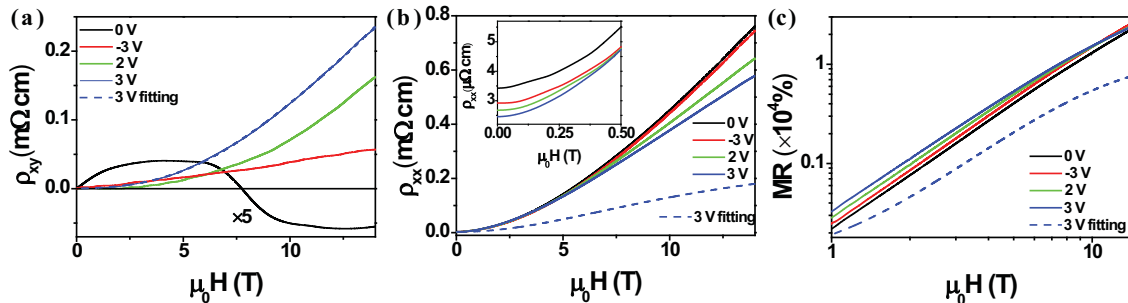


FIG. 4. The magnetic-field dependence of (a)  $\rho_{xy}$ , (b)  $\rho_{xx}$ , and (c) MR at 2 K at various electrolytic gate voltages shown in the legend. The inset in (b) shows  $\rho_{xx}$  at a low field. The blue dashed lines in (a)–(c) are fits to the two-band model Eqs. (1) and (2) for  $V_g = 3$  V as described in the text.

Figure 4 shows the Hall resistivity and magnetoresistance of a second  $\text{WTe}_2$  device with a thickness of  $\sim 70$  nm, tuned by electrolyte gating [14]. As shown in Fig. 4(a), the  $\rho_{xy}(H)$  curve at  $V_g = 0$  V is highly nonlinear with holes dominating at the high field. After applying a positive gate voltage, the  $\rho_{xy}(H)$  is uniformly positive (electronlike). Applying a negative gate voltage had little effect. The electron doping at the positive gate voltage is irreversible, persisting after returning the device to  $V_g = 0$  V (see Supplemental Material Fig. S4 [13]). These observations are consistent with irreversible doping due to the intercalation of donor Li ions into the spacing layer between Te atoms [20] at positive gate voltages. The Hall resistivity at  $V_g = 3$  V can be well fit with Eq. (2) with the constraint of  $\rho_{xx}(0) = \frac{1}{e(n\mu + p\mu')}$  yielding  $n_e = 1.36 \times 10^{20} \text{ cm}^{-3}$  and  $p/n = 0.84$ , suggesting  $\text{WTe}_2$  has become strongly electron doped. Notably the mobility is only slightly reduced upon gating (at  $V_g = 0, \mu = 2.25 \text{ m}^2 \text{ V}^{-1} \text{ s}^{-1}$ , and  $\mu' = 0.92 \text{ m}^2 \text{ V}^{-1} \text{ s}^{-1}$ ; after gating,  $\mu = 1.19 \text{ m}^2 \text{ V}^{-1} \text{ s}^{-1}$  and  $\mu' = 0.82 \text{ m}^2 \text{ V}^{-1} \text{ s}^{-1}$ ) indicating that insertion of Li ions introduces little disorder. Figure 4(b) presents  $\rho_{xx}(H)$  at various gate voltages; the  $\rho_{xx}$  value decreases with increasing doping. Interestingly, a large magnetoresistance was also observed in electron-doped  $\text{WTe}_2$  with no evidence of saturation up to 14 T;  $\rho_{xx}(H)$  is never sublinear in  $H$ . Although  $\rho_{xx}(H = 14 \text{ T})$

is lower at  $V_g = 3$  V (high electron doping), compared to  $V_g = 0$  V, it should be noted that  $\rho_{xx}(0)$  also decreases with increasing doping as shown in the inset of Fig. 4(b). Figure 4(c) shows the field dependence of MR at various gate voltages, and the MR is slightly gate dependent and is in fact even larger in the electron-doped  $\text{WTe}_2$  ( $V_g = 3$  V) compared to  $V_g = 0$  V over the measured field range of  $H \leq 14$  T (see Supplemental Material Fig. S4 [13]). In the case of graphite and bismuth, MR tends to saturate when  $H$  exceeds several teslas because of the slight deviation in the perfect compensation of electrons and holes [21,22]. Notably the  $p/n$  ratio different than 1 at  $V_g = 3$  V predicts a saturating MR [ $\rho_{xx}(H)$  is sublinear in  $H$  for  $H > 11$  T] as shown in the blue dashed line in Figs. 4(b) and 4(c), which is not observed in the experiment. The large MR in  $\text{WTe}_2$  persists even when electrons and holes are not compensated as determined by the Hall effect and electrolyte gating effect, which suggest that perfect electron-hole compensation is not necessary for the XMR in  $\text{WTe}_2$ , and other mechanisms should be considered [5,23].

Materials synthesis efforts were supported by the Gordon and Betty Moore Foundation Grant No. GBMF4419. M.S.F. is supported by Australian Research Council Grant No. DP150103837.

- 
- [1] S. Z. Butler, S. M. Hollen, L. Cao, Y. Cui, J. A. Gupta, H. R. Gutiérrez, T. F. Heinz, S. S. Hong, J. Huang, A. F. Ismach, E. Johnston-Halperin, M. Kuno, V. V. Plashnitsa, R. D. Robinson, R. S. Ruoff, S. Salahuddin, J. Shan, L. Shi, M. G. Spencer, M. Terrones, W. Windl, and J. E. Goldberger, *ACS Nano* **7**, 2898 (2013).
- [2] M. N. Ali, J. Xiong, S. Flynn, J. Tao, Q. D. Gibson, L. M. Schoop, T. Liang, N. Haldolaarachchige, M. Hirschberger, N. P. Ong, and R. J. Cava, *Nature (London)* **514**, 205 (2014).
- [3] X. Du, S.-W. Tsai, D. L. Maslov, and A. F. Hebard, *Phys. Rev. Lett.* **94**, 166601 (2005).
- [4] I. Pletikosić, M. N. Ali, A. V. Fedorov, R. J. Cava, and T. Valla, *Phys. Rev. Lett.* **113**, 216601 (2014).
- [5] J. Jiang, F. Tang, X. C. Pan, H. M. Liu, X. H. Niu, Y. X. Wang, D. F. Xu, H. F. Yang, B. P. Xie, F. Q. Song, P. Dudin, T. K. Kim, M. Hoesch, P. K. Das, I. Vobornik, X. G. Wan, and D. L. Feng, *Phys. Rev. Lett.* **115**, 166601 (2015).
- [6] Z. Zhu, X. Lin, J. Liu, B. Fauqué, Q. Tao, C. Yang, Y. Shi, and K. Behnia, *Phys. Rev. Lett.* **114**, 176601 (2015).
- [7] D. Rhodes, S. Das, Q. R. Zhang, B. Zeng, N. R. Pradhan, N. Kikugawa, E. Manousakis, and L. Balicas, *Phys. Rev. B* **92**, 125152 (2015).
- [8] P. L. Cai, J. Hu, L. P. He, J. Pan, X. C. Hong, Z. Zhang, J. Zhang, J. Wei, Z. Q. Mao, and S. Y. Li, *Phys. Rev. Lett.* **115**, 057202 (2015).
- [9] D. Kang, Y. Zhou, W. Yi, C. Yang, J. Guo, Y. Shi, S. Zhang, Z. Wang, C. Zhang, S. Jiang, A. Li, K. Yang, Q. Wu, G. Zhang, L. Sun, and Z. Zhao, *Nat. Commun.* **6**, 7804 (2015).
- [10] X.-C. Pan, X. Chen, H. Liu, Y. Feng, Z. Wei, Y. Zhou, Z. Chi, L. Pi, F. Yen, F. Song, X. Wan, Z. Yang, B. Wang, G. Wang, and Y. Zhang, *Nat. Commun.* **6**, 7805 (2015).
- [11] Y. Luo, H. Li, Y. M. Dai, H. Miao, Y. G. Shi, H. Ding, A. J. Taylor, D. A. Yarotski, R. P. Prasankumar, and J. D. Thompson, *Appl. Phys. Lett.* **107**, 182411 (2015).
- [12] C.-H. Lee, E. C. Silva, L. Calderin, M. A. T. Nguyen, M. J. Hollander, B. Bersch, T. E. Mallouk, and J. A. Robinson, *Sci. Rep.* **5**, 10013 (2015).
- [13] See Supplemental Material at <http://link.aps.org/supplemental/10.1103/PhysRevB.93.121108> for additional data.
- [14] D. Kim, S. Cho, N. P. Butch, P. Syers, K. Kirshenbaum, S. Adam, J. Paglione, and M. S. Fuhrer, *Nat. Phys.* **8**, 459 (2012).
- [15] Y. Zhao, H. Liu, J. Yan, W. An, J. Liu, X. Zhang, H. Wang, Y. Liu, H. Jiang, Q. Li, Y. Wang, X.-Z. Li, D. Mandrus, X. C. Xie, M. Pan, and J. Wang, *Phys. Rev. B* **92**, 041104 (2015).
- [16] L. R. Thoutam, Y. L. Wang, Z. L. Xiao, S. Das, A. Luican-Mayer, R. Divan, G. W. Crabtree, and W. K. Kwok, *Phys. Rev. Lett.* **115**, 046602 (2015).
- [17] K. Wang, D. Graf, L. Li, L. Wang, and C. Petrovic, *Sci. Rep.* **4**, 7328 (2014).
- [18] Z. J. Xiang, G. J. Ye, C. Shang, B. Lei, N. Z. Wang, K. S. Yang, D. Y. Liu, F. B. Meng, X. G. Luo, L. J. Zou, Z. Sun, Y. Zhang, and X. H. Chen, *Phys. Rev. Lett.* **115**, 186403 (2015).
- [19] C. M. Hurd, *The Hall Effect in Metals and Alloys, The International Cryogenics Monograph Series* (Springer, Berlin, 1972).
- [20] Y. Yu, F. Yang, X. F. Lu, Y. J. Yan, H. ChoYong, L. Ma, X. Niu, S. Kim, Y.-W. Son, D. Feng, S. Li, S.-W. Cheong, X. H. Chen, and Y. Zhang, *Nat. Nanotechnol.* **10**, 270 (2015).
- [21] Y. Kopelevich, J. H. S. Torres, R. R. da Silva, F. Mrowka, H. Kempa, and P. Esquinazi, *Phys. Rev. Lett.* **90**, 156402 (2003).
- [22] F. Benoît, V. Baptiste, P. Cyril, I. Jean-Paul, and B. Kamran, *New J. Phys.* **11**, 113012 (2009).
- [23] M. M. Parish and P. B. Littlewood, *Nature (London)* **426**, 162 (2003).